AIMS Mathematics, 11(4): 10963–10985.
DOI: 10.3934/math.2026450
Received: 18 February 2026
Revised: 05 April 2026
Accepted: 08 April 2026
Published: 20 April 2026

https://www.aimspress.com/journal/Math

Research article

Modeling and estimation in aquaculture ponds based on bioenergetic fish growth models

Sharefa Asiri*, Salma Al-Tuwairqi and Sara Al-Amoudi

Department of Mathematics, King Abdulaziz University, Jeddah 1540, Saudi Arabia

* **Correspondence:** Email: smaasiri@kau.edu.sa.

Abstract: Aquaculture is a vital component in meeting the increasing demand for food by providing a sustainable alternative to traditional sources that are no longer sufficient to cover future needs. In this paper, we focused on studying the fundamental factors influencing the performance of aquaculture systems, where the accumulation of unionized ammonia (UIA) represents one of the most critical challenges directly affecting fish health, growth, and population density within ponds. In this work, a bioenergetic mathematical model for fish growth was developed to accurately represent the system dynamics through the integration of UIA effects and their relationship with total fish biomass (ξ) and fish population (P). The model was analyzed using qualitative mathematical tools to verify the positivity and boundedness of the state variables, determine equilibrium points, and assess their stability. Moreover, numerical simulations were performed to capture the growth dynamics under different conditions. In addition, the modulating function method was applied to estimate the UIA concentration.

Keywords: aquaculture; mathematical model; bioenergetic growth; unionized ammonia; stability analysis; modulating function method
Mathematics Subject Classification: 34Dxx, 91-10, 81P50

1. Introduction

Aquaculture is the farming of aquatic organisms such as fish, crustaceans, mollusks, and aquatic plants. It is similar to agriculture, but with fish instead of plants or livestock. Fisheries are vital to the global food supply and are becoming critical components of countries' economies. The Food and Agriculture Organization stated that the fishery products deficit will reach 29 million tons in 2030 [1]. According to the UN, by 2050, there will be 9.7 billion people on the planet, which cannot be covered by wild capture. Therefore, the fishery market is turning toward aquaculture production, which has become a key provider of seafood and a crucial element for sustainable food production.

Fish growth is a complex process driven by biological interactions and is a key determinant of fish life history. In aquaculture, growth is a critical trait, alongside environmental and management factors, that influences production outcomes [2]. The growth and health of fish are affected by feeding and water quality factors. The feeding factors involve feeding time, rate, and frequency. Water quality is important for the success of fish farming [3]; however, it is the hardest to control. High water quality means more profit, less mortality, and increased productivity in fish ponds. Thus, the key to the success or failure of the fish farming process is the quality of the water in the fish farm. This is because water is the medium (environment) in which fish live and carry out all their vital processes, such as feeding, breathing, excretion, and reproduction. The major factors affecting water quality are temperature, dissolved oxygen (DO), potential of hydrogen (pH), and unionized ammonia (UIA) [3]. In aquaculture systems, monitoring ammonia concentration in water is of critical importance due to its direct impact on aquatic animal health and the sustainability of production environments.

Several researchers have analyzed parameters such as DO, ammonia concentration, pH, and temperature regulation. Darmawan et al. showed that aeration systems play a vital role in maintaining DO at optimal levels while reducing stress and mortality in fish [4]. Similarly, Satanwat highlighted the effects of ammonia on fish growth and immune response, stressing the importance of biofiltration and regular monitoring of water [5]. Batır et al. emphasized the role of land-based integrated multi-trophic aquaculture systems in cycling nutrients and promoting balanced ecosystems [6]. Tabrett et al. demonstrated the benefits of aquatic plants in nutrient removal and pond health improvement [7]. Flores-Iwasaki et al. showed that improved water monitoring increases growth rates and reduces culture mortality [8].

A bioenergetic model has been developed to describe the growth rate of fish depending on the nutrition, temperature, and weight of the fish [9]. Then the concept of fish growth evolved into the processes of anabolism and catabolism [10].

In 2000, a bioenergetic model was developed by involving DO [11]. This shows that the DO concentration affects the food consumption, metabolic rate, and energy; hence, it affects the fish's weight. In 2010, the fish stocking density was added to the model, which gave a better understanding of fish growth and feed efficiency [12]. In 2023, Aljehani et al. developed the bioenergetic models by considering the density population dynamics [13]. The fish population dynamic model includes the fish stocking density and mortality rate. Then, the same authors proposed a new version of the fish population growth model, which includes the fish population and dissolved oxygen dynamics [14].

Ammonia accumulation remains a critical factor limiting fish growth, survival rates, and farm profitability. Fish waste and uneaten food generate significant amounts of ammonia, which is highly toxic to aquatic species; this leads to physiological stress, increased mortality, and reduced feed efficiency. Biological filtration methods, while traditional, can be highly effective at reducing ammonia shock toxicity, depending on system design, species selection, and environmental conditions. However, the direct influence of ammonia concentration on metabolic processes is overlooked in current bioenergetic models commonly used for fish growth prediction. Most models focus on food efficiency, temperature regulation, and DO levels, while not integrating ammonia as a dynamic variable in the fish growth in a fully interdependent manner. Given the rapid development of aquaculture technology, it is essential to design an improved mathematical model that treats ammonia concentration as the primary determinant of fish growth. In this research, a dynamic bioenergetic model is developed to bridge this gap by taking into account environmental conditions, particularly

the ammonia concentration, and optimizing the efficiency of fish farming. More specifically, we extend the bioenergetic model in [13] by incorporating UIA dynamics into the dynamical system, thereby providing deeper insight into the relationships among ammonia concentration, fish weight, and population density. Having such a model enables managers to simulate growth outcomes under varying conditions without the risks of real-world trial and error. In addition, the model helps aquaculture managers in, e.g., optimizing feeding regimes, determining the maximum sustainable carrying capacity of the system, and the required filtration capacity.

In addition, the modulating function method (MFM) is used to estimate the UIA concentration (see [15–17]). Estimating UIA can serve as a robust soft sensor for automated water-quality control.

The MFM relies directly on the original mathematical model, enabling accurate estimation without simplifications or approximations. Moreover, it does not require prior knowledge of the system's initial conditions, making it particularly suitable for problems where these conditions are unknown or difficult to determine precisely. One of its key strengths is that it avoids numerical differentiation of noisy data, thereby significantly reducing the impact of noise and measurement errors on the results [18].

The contributions of this paper are:

i) Develop a comprehensive bioenergetic model to understand fish behavior, movement patterns, and population dynamics under varying environmental conditions. The model integrates essential biological and environmental factors, particularly the effects of UIA, temperature, and DO, to accurately represent the metabolic processes that govern fish growth and mortality.

ii) Provide a qualitative and stability analysis to examine the relationship between UIA concentration, fish biomass, and population density. The analysis verifies the positivity, boundedness, and local asymptotic stability of the system, ensuring that the model remains biologically realistic and mathematically consistent.

iii) Apply the MFM to estimate UIA in noise-free and noisy data cases.

The paper is organized as follows: In Section 2, we develop a bioenergetic model by integrating ammonia dynamics. In Section 3, we qualitatively analyze the model, identifying the positive and bounded region of state variables, determining steady-state solutions, and examining their stability. Numerical simulations are conducted, and parameter sensitivity analysis is performed in Section 4. In Section 5, we discuss the application of the MFM to estimate the UIA concentration. Then, the robustness of the method is demonstrated numerically in Section 6, where noise-free and noisy cases are considered. Finally, the key findings of this paper and the directions for future work are presented in Section 7.

2. Mathematical model

The dynamics of fish population growth in ponds can be described using the bioenergetic model. This model considers the fish's metabolism and environmental factors that can affect the growth and survival of the fish population. The proposed model is divided into three state variables: The total fish biomass ($\xi(t)$), the total fish number ($P(t)$), and the concentration of unionized ammonia ($U(t)$). These variables change over time and are influenced by different factors, which we will describe in detail.

To understand the dynamics of the system, we need to make some assumptions. First, we assume that the fish pond is stocked with a certain number of fish (p_s), each with an individual biomass (ξ_i). The amount of fish food available in the pond is a crucial factor affecting fish anabolism. The anabolism

rate is expressed by the term $b\Psi(f, T, DO)(1 - U)$, where b is the anabolism rate. $\Psi(f, T, DO)$ is a function of the amount of fish food (f), water temperature (T), and dissolved oxygen (DO) in the pond. The presence of unionized ammonia (U) in the pond affects the percentage of fish anabolism. When the concentration of unionized ammonia is high, the percentage of fish anabolism decreases, leading to slower growth and reproduction rates [19]. The term $(1 - U)$ represents a first-order inhibitory effect, providing a mathematically tractable and transparent way to model the reduction in metabolic efficiency without introducing additional parameters.

In addition, we assume that some water temperature levels and the percentage of unionized ammonia due to the fish population are factors in fish catabolism that lead to mortality [20]. Fish biomass decays due to catabolism function $k(T)$, at a rate of d_1, and due to population unionized ammonia, at a rate of d_2. We also assume that the fish population decays due to unionized ammonia at a rate of d_3. When the concentration of unionized ammonia in the pond is high, fish mortality increases, leading to a decline in the fish population.

The concentration of unionized ammonia in the pond increases due to the fish population at a rate of c_1 and due to the catabolism function $k(T)$ at a rate of c_2. Furthermore, the pond filtering systems reduce the concentration of unionized ammonia at a rate of r. The filtering systems play a crucial role in maintaining the pond's water quality, which directly impacts the survival and growth of the fish population.

The dynamics of the model are governed by the following nonlinear system of ordinary differential equations (ODEs) (2.1), which describes how the state variables change over time and how they are influenced by the factors we have discussed:

$$\begin{cases} \dfrac{\mathrm{d}\xi}{\mathrm{d}t} = p_s\xi_i + b\Psi(f, T, DO)(1 - U)\xi - d_1k(T)\xi - d_2PU\xi, & \text{(2.1a)} \\ \dfrac{\mathrm{d}P}{\mathrm{d}t} = p_s - d_3PU, & \text{(2.1b)} \\ \dfrac{\mathrm{d}U}{\mathrm{d}t} = c_1PU + c_2k(T)U - rU. & \text{(2.1c)} \end{cases}$$

The variables and parameters used in the model are summarized in Table 1. The values of model-specific rate parameters, b, d_1, d_2, d_3, c_1, c_2, and r, are between 0 and 1.

3. Qualitative analysis

We study model (2.1) qualitatively. First, we determine the positive and bounded region for the state variables, and then we obtain the steady-state solutions of the model and examine their stability [21]. The major results are given in the following theorems:

Theorem 1. *If $\xi(0) > 0$, $P(0) > 0$ and $U(0) \geq 0$, then the set*

$$\Gamma = \{(\xi, P, U) \in R^3_{\geq 0}, 0 < \xi \leq L_1, 0 < P \leq L_2, 0 \leq U \leq L_3\}$$

is positively invariant where

$$L_1 = \left(\xi(0) + \frac{p_s\xi_i}{b\Psi}\right)e^{b\Psi z_1}, \quad L_2 = P(0) + p_sz_2, \quad \text{and} \quad L_3 = U(0)\exp\left((c_1L_2 + c_2k(T))\, z_3\right),$$

whereas $z_1, z_2, z_3 \in [0, H]$, and H is any number.

Table 1. Nomenclature and major parameters of the growth model [9].

Symbol	Description	Unit
t	Time	day
ξ	Total fish biomass	kcal/pond
P	Total fish number	fish/pond
U	Unionized ammonia	mg/l (UIA)
T	Temperature	°C
DO	Dissolved oxygen	mg/l
p_s	Stocking fish number	fish/day/pond
ξ_i	Individual fish biomass during fish stocking	kcal/fish
Ψ	Anabolism function	-
k	Catabolism function	-
f	Relative feeding rate	day^{-1}
b	Anabolism rate	day^{-1}
d_1	Catabolism rate due to temperature	day^{-1}
d_2	Catabolism rate due to UIA	day^{-1}
d_3	Mortality rate of population due to UIA	day^{-1}
c_1	Rate of UIA due to population	day^{-1}
c_2	Rate of UIA due to temperature	day^{-1}
r	Rate of filtering UIA	day^{-1}

Proof. From Eq (2.1a), we conclude the inequality

$$\frac{\mathrm{d}\xi}{\mathrm{d}t} \geqslant -d_1 k(T)\xi - d_2 PU\xi = \nu_1(P,U)\xi,$$

where

$$\nu_1(P,U) = -d_1 k(T) - d_2 PU.$$

Thus,

$$\frac{\mathrm{d}\xi}{\xi} \geqslant \nu_1(P,U)dt.$$

Integration over $[0,t]$ gives

$$\ln(\xi)|_0^t \geqslant \int_0^t \nu_1 dt.$$

Substituting for the limits of integration, we get

$$\ln\xi(t) - \ln\xi(0) \geqslant \int_0^t \nu_1 dt,$$
$$\ln\left(\frac{\xi(t)}{\xi(0)}\right) \geqslant \int_0^t \nu_1 dt.$$

By taking the exponential function of both sides, we have

$$\xi(t) \geqslant \xi(0) \exp\left(\int_0^t \nu_1 dt\right) > 0,$$

since $\xi(0) > 0$ and the exponential function is always positive.

From Eq (2.1b), we note that

$$\frac{dP}{dt} \geqslant -d_3 PU = P\nu_2(U).$$

Then by separating the variables, we obtain

$$\frac{dP}{P} \geqslant \nu_2 dt,$$

where

$$\nu_2(U) = -d_3 U.$$

Integration over $[0, t]$ gives

$$P(t) \geqslant P(0) \exp\left(\int_0^t \nu_2 dt\right) > 0,$$

since $P(0) > 0$ and the exponential function is always positive.

Similarly, from Eq (2.1c), we can write the following inequality

$$\frac{dU}{dt} \geqslant c_2 k(T)U - rU = (c_2 k(T) - r)\, U.$$

Hence,

$$\frac{dU}{U} \geqslant (c_2 k(T) - r)\, dt.$$

Integration over $[0, t]$ gives

$$U(t) \geqslant U(0) \exp\left((c_2 k(T) - r)\, t\right) > 0.$$

Additionally, since $U(0) \geqslant 0$, we have $U(t) \geqslant 0$. Hence, the solution (ξ(t), P(t), U(t)) is nonnegative for nonnegative initial data. Next, we prove that all solutions will remain bounded. We start by rewriting the first Eq (2.1a) as follows:

$$\frac{\mathrm{d}\xi}{\mathrm{d}t} \leqslant p_s \xi_i + b\Psi\xi,$$
$$\frac{\mathrm{d}\xi}{\mathrm{d}t} - b\Psi\xi \leqslant p_s \xi_i.$$

The integrating factor to the previous inequality is

$$\mu = e^{-\int b\Psi dt} = e^{-b\Psi t}.$$

Multiplying the inequality by the integrating factor, we obtain

$$\frac{d}{dt}\left(e^{-b\Psi t}\xi\right) \leqslant e^{-b\Psi t} p_s \xi_i.$$

Integration over $[0, t]$ gives

$$\begin{aligned} e^{-b\Psi t}\xi\big|_0^t &\leqslant \int_0^t e^{-b\Psi t} p_s \xi_i dt, \\ e^{-b\Psi t}\xi(t) - \xi(0) &\leqslant p_s\xi_i \left(\frac{e^{-b\Psi t}}{-b\Psi}\right)_0^t \\ &= p_s\xi_i \left(\frac{e^{-b\Psi t}}{-b\Psi} + \frac{1}{b\Psi}\right) \\ &= \frac{p_s\xi_i}{b\Psi}\left(1 - e^{-b\Psi t}\right). \end{aligned}$$

Then,

$$\begin{aligned} \xi(t) &\leqslant \xi(0)e^{b\Psi t} + \frac{p_s\xi_i}{b\Psi}e^{b\Psi t} - \frac{p_s\xi_i}{b\Psi}, \\ \xi(t) &\leqslant \left(\xi(0) + \frac{p_s\xi_i}{b\Psi}\right)e^{b\Psi z_1} = L_1, \end{aligned}$$

where $z_1 \in [0, H]$, and H is any number.

Rewrite the second Eq (2.1b) as follows:

$$\frac{dP}{dt} \leqslant p_s.$$

Integration over $[0, t]$ gives

$$\begin{aligned} P(t)|_0^t &\leqslant \int_0^t p_s dt, \\ P(t) - P(0) &\leqslant p_s t, \\ P(t) &\leqslant P(0) + p_s z_2 = L_2, \end{aligned}$$

where $z_2 \in [0, H]$, and H is any number.

Again, rewriting the third Eq (2.1c) as

$$\frac{dU}{dt} \leqslant (c_1 P + c_2 k(T))\, U.$$

Since $P \leqslant L_2$, we have

$$\frac{dU}{dt} \leqslant (c_1 L_2 + c_2 k(T))\, U.$$

Integration over $[0, t]$ gives

$$\begin{aligned} \frac{dU}{U} &\leqslant (c_1 L_2 + c_2 k(T))\, dt, \\ U(t) &\leqslant U(0) \exp\left((c_1 L_2 + c_2 k(T))\, z_3\right) = L_3, \end{aligned}$$

where $z_3 \in [0, H]$, and H is any number.

Hence, the state variables (ξ(t), P(t), U(t)) are bounded for all t. □

Theorem 2. *The model has a unique equilibrium point*

$$E^* = (\xi^*, P^*, U^*)$$

if $R_1 > 1$ *and* $R_2 > 1$, *where*

$$\begin{aligned}
\xi^* &= \frac{p_s \xi_i}{d_1 k(T) + d_2 P^* U^* - b\Psi\,(1 - U^*)}, \\
P^* &= \frac{1}{c_1}\,(r - c_2 k(T))\,, \\
U^* &= \frac{c_1 p_s}{d_3\,(r - c_2 k(T))}, \\
R_1 &= \frac{r}{c_2 k(T)},
\end{aligned}$$

and

$$R_2 = \frac{d_1 k(T) + d_2 P^* U^*}{b\Psi(1 - U^*)}.$$

Proof. The equilibrium points of the system are the steady-state solutions obtained by setting the rates of the equations in (2.1) to zero:

$$p_s \xi_i + b\Psi(f, T, DO)(1 - U)\xi - d_1 k(T)\xi - d_2 PU\xi = 0, \tag{3.1}$$

$$p_s - d_3 PU = 0, \tag{3.2}$$

$$c_1 PU + c_2 k(T)U - rU = 0. \tag{3.3}$$

From Eq (3.3), $U \neq 0$; hence,

$$c_1 P + c_2 k(T) - r = 0.$$

Thus,

$$P^* = \frac{1}{c_1 c_2 k(T)}\left(\frac{r}{c_2 k(T)} - 1\right) = \frac{1}{c_1 c_2 k(T)}\,(R_1 - 1)\,, \tag{3.4}$$

where P^* is positive if $R_1 > 1$.

From Eq (3.2), one can write

$$U = \frac{p_s}{d_3}\frac{1}{P}. \tag{3.5}$$

By substituting Eq (3.4) into Eq (3.5), we have

$$U^* = \frac{c_1 p_s}{d_3\,(r - c_2 k(T))},$$

where U^* is positive if $R_1 > 1$.

By solving Eq (3.1) for ξ and using P^*, U^*, we get

$$\xi^* = \frac{p_s \xi_i}{b\Psi\,(1 - U^*)\,(\frac{d_1 k(T) + d_2 P^* U^*}{b\Psi\,(1 - U^*)} - 1)} = \frac{p_s \xi_i}{b\Psi\,(1 - U^*)\,(R_2 - 1)}$$

where ξ^* is positive if $R_2 > 1$.

Hence, a unique equilibrium point exists under the given conditions. □

The next theorem will prove the stability of the equilibrium point of model (2.1) by using the linearization method [21].

Theorem 3. *The equilibrium point E^* is locally asymptotically stable if it exists.*

Proof. The Jacobian matrix of model (2.1) at E^* is given by

$$J(E^*) = \begin{pmatrix} b\Psi(1-U^*) - d_1k(T) - d_2P^*U^* & -d_2U^*\xi^* & -b\Psi\xi^* - d_2P^*\xi^* \\ 0 & -d_3U^* & -d_3P^* \\ 0 & c_1U^* & c_1P^* + c_2k(T) - r \end{pmatrix}. \tag{3.6}$$

Solving the characteristic equation

$$|J(E^*) - \lambda I| = 0,$$

we get

$$(b\Psi(1-U^*) - d_1k(T) - d_2P^*U^* - \lambda)\left[(-d_3U^* - \lambda)(c_1P^* + c_2k(T) - r - \lambda) + c_1d_3U^*P^*\right] = 0.$$

Then,

$$b\Psi(1-U^*) - d_1k(T) - d_2P^*U^* - \lambda = 0$$

or

$$(-d_3U^* - \lambda)(c_1P^* + c_2k(T) - r - \lambda) + c_1d_3U^*P^* = 0.$$

From the first equation, we have

$$\lambda_1 = b\Psi(1-U^*) - d_1k(T) - d_2P^*U^*.$$

For λ_1 to be negative

$$d_1k(T) + d_2P^*U^* > b\Psi(1-U^*),$$

that is, $R_2 > 1$, this is satisfied since this condition is a condition for the existence of E^*.

From the second equation, we obtain

$$a\lambda^2 + b\lambda + c = 0,$$

where

$$a = 1, \tag{3.7}$$

$$b = d_3U^* - c_1P^* - c_2k(T) + r, \tag{3.8}$$

$$c = -d_3U^*(c_1P^* + c_2k(T) - r) + c_1d_3U^*P^*. \tag{3.9}$$

Clearly, we can see that $a > 0$. Now, in Eq (3.8), we will substitute U^* and P^* with their values to obtain

$$b = \frac{c_1p_s}{r - c_2k(T)} + 2(r - c_2k(T)).$$

Since the equilibrium point exists if $R_1 > 1$, that is, $r > c_2k(T)$, this means that $b > 0$.

Additionally, from Eq (3.9), we have

$$c = 0 + c_1 d_3 U^* P^*,$$

since

$$(c_1 P^* + c_2 k(T) - r) = 0.$$

Therefore,

$$c = c_1 d_3 U^* P^* > 0.$$

Because $a, b, c > 0$, all eigenvalues are negative. Therefore, E^* is locally asymptotically stable if it exists. □

4. Numerical analysis

We solve system (2.1) numerically and illustrate simulations of the model using ode45, a solver in MATLAB for ODEs. Then we conduct numerical experiments to show the agreement with the qualitative results. We explore the sensitivity of the parameters to gain more insight into those critical parameters that may lead to improving the aquaculture process. The values of the parameters are taken from Table 2, where they have been selected such that the conditions of Theorems 2 and 3 are satisfied. Thus, equilibrium E^* exists and exhibits local asymptotic stability.

Table 2. Parameter values.

Parameter	p_s	ξ_i	b	d_1	d_2	d_3	c_1	c_2	r
Value	2	30	0.5	0.03	0.05	0.05	0.08	0.09	1

4.1. Numerical experiments

We solve model (2.1) numerically with the following different initial values:

$$\begin{aligned}
&(IC1)\ \ \xi(0) = 60, \quad P(0) = 30, \quad U(0) = 0.1;\\
&(IC2)\ \ \xi(0) = 120, \ P(0) = 60, \quad U(0) = 0.2;\\
&(IC3)\ \ \xi(0) = 180, \ P(0) = 90, \quad U(0) = 0.3;\\
&(IC4)\ \ \xi(0) = 240, \ P(0) = 120, \ U(0) = 0.4.
\end{aligned}$$

We set the parameters as in Table 2, taking into account the conditions in Theorem 2. Figure 1 demonstrates how the state variables change over time. We find that they fluctuate but reach equilibrium, where the equilibrium values are $\xi = 18.2501$, $P = 11.3750$, and $U = 3.5165$. The figure also shows that these equilibrium values are the same no matter how the initial conditions change. By qualitatively calculating the equilibrium point from Theorem 2 with the same parameters, we obtain equilibrium point E^*=(18.8065, 11.9375, 3.3508). Therefore, the qualitative results are consistent with the numerical results.

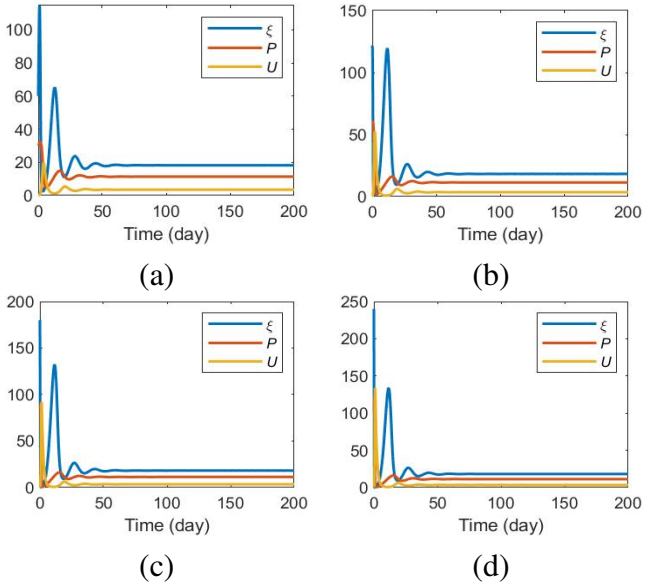

Figure 1. Time variation in the total fish biomass, the fish population, and UIA of the model with initial values (IC1)–(IC4). The parameter values are given in Table 2.

Next, we change some parameter values and compare the numerical and qualitative results. In Figure 2, we change the catabolism rate due to temperature to $d_1 = 0.09$, the mortality rate of the population due to UIA to $d_3 = 0.08$, and the rate of UIA due to temperature to $c_2 = 0.02$. We find that the equilibrium values reach the following values: $\xi = 32.2534$, $P = 12.2500$, and $U = 2.0408$. This equilibrium point is very close to the equilibrium point in the qualitative calculations, that is, E^*=(33.239, 12.3750, 2.0202).

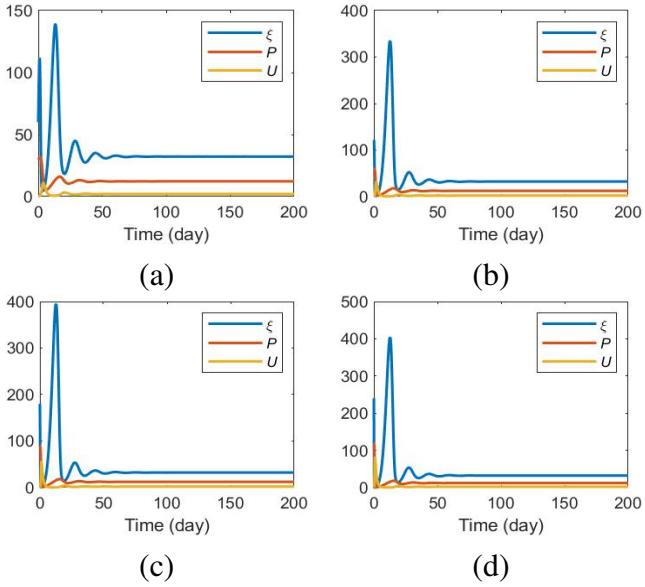

Figure 2. Time variation in the total fish biomass, the fish population, and UIA of the model with initial values (IC1)–(IC4). The parameter values are: $b = 0.5$, $a = 0.5$, $d_1 = 0.09$, $d_2 = 0.05$, $d_3 = 0.08$, $c_1 = 0.08$, $c_2 = 0.02$, and $r = 1$.

Similarly, in Figure 3, we change the catabolism rate due to temperature to $d_1 = 0.02$, the catabolism rate due to UIA to $d_2 = 0.04$, the mortality rate of the population due to UIA to $d_3 = 0.03$, the rate of UIA due to population to $c_1 = 0.05$, and the rate of UIA due to temperature to $c_2 = 0.02$. We find that the equilibrium values reach the following values: $\xi = 15.0147$, $P = 18.4004$, and $U = 3.6230$. This equilibrium point is very close to the equilibrium point in the qualitative calculations, that is, E^*=(15.3344, 19.2000,3.4722). Hence, we can say that the numerical and qualitative results are in good agreement. Figures 1–3 numerically demonstrate that the equilibrium point is globally asymptotically stable.

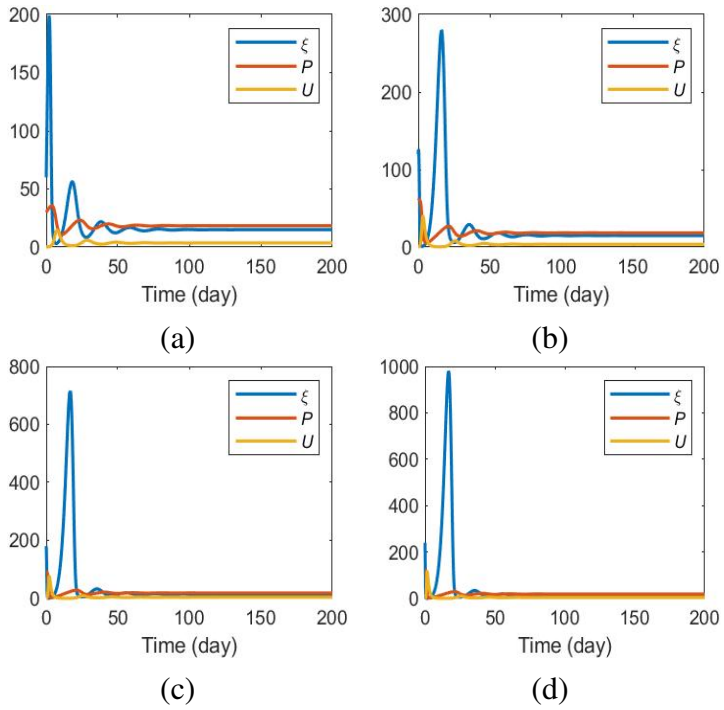

Figure 3. Time variation in the total fish biomass, the fish population, and UIA of the model with initial values (IC1)–(IC4). The parameter values are: $b = 0.5$, $a = 0.5$, $d_1 = 0.02$, $d_2 = 0.04$, $d_3 = 0.03$, $c_1 = 0.05$, $c_2 = 0.08$, and $r = 1$.

If we repeat the last experiment with $r = 0.03$, so that the first condition ($R_1 > 1$) of Theorem 2 is not satisfied, Figure 4 shows that the system loses stability. The fish-biomass and fish-number solutions decay to zero, while the UIA solution diverges. This behavior is expected: A sharp decline in the UIA-filtering rate r produces a marked increase in U, which in turn causes a pronounced decline in fish biomass ξ, leading to mortality.

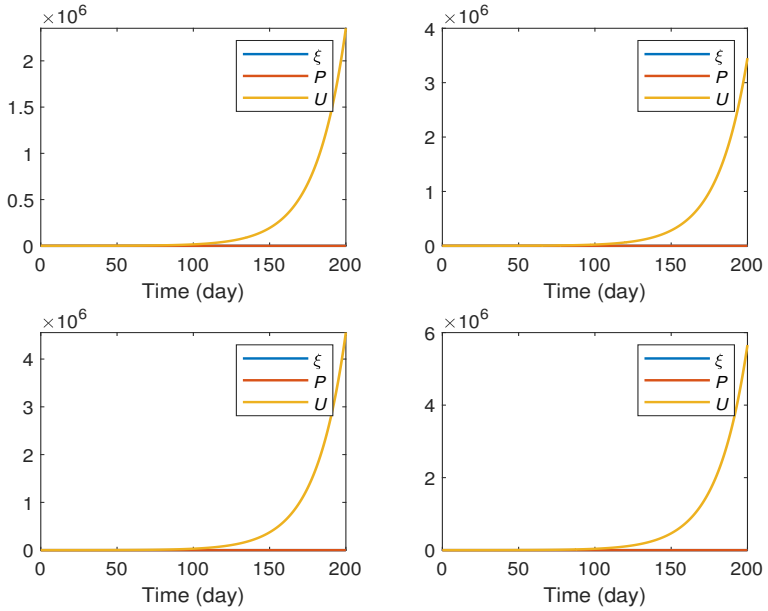

Figure 4. Time variation in the total fish biomass, the fish population, and UIA of the model with initial values (IC1)–(IC4). The parameter values are: $b = 0.5$, $a = 0.5$, $d_1 = 0.02$, $d_2 = 0.04$, $d_3 = 0.03$, $c_1 = 0.05$, $c_2 = 0.08$, and $r = 0.03$.

4.2. Parameter analysis

We set four values for each parameter presented in Table 2 and study their effect on the fish biomass, the fish population, and the concentration of UIA. In all figures, we use the initial condition (IC1).

The result presented in Figure 5a highlights the effect of the anabolism rate b on fish biomass. The graph shows that as the rate of anabolism increases, fish biomass initially increases, resulting in more fish waste. This fish waste leads later to a decrease in biomass as anabolism increases, driven by a rise in UIA over a specific period, as shown in Figure 5c. The resulting rise in UIA introduces a metabolic drag on the system. In Figure 5b,c, we also note that UIA and fish number remain relatively invariant to changes in b.

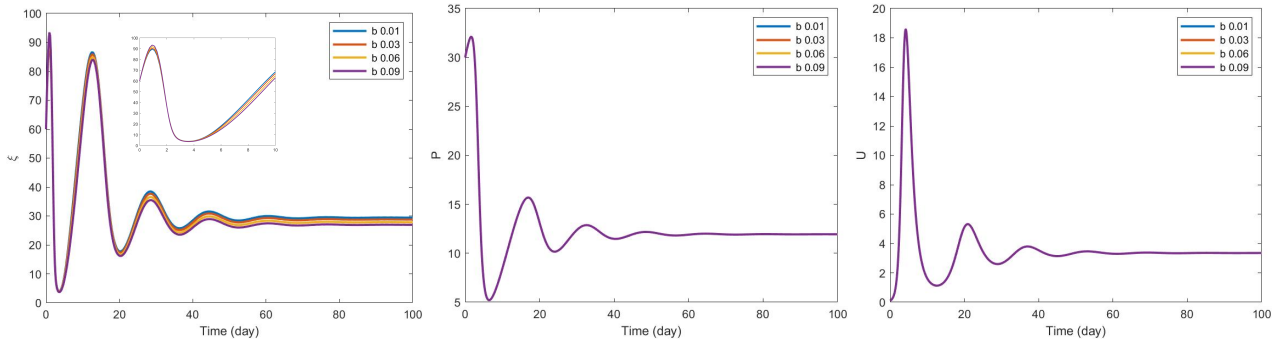

(a) **(b)** **(c)**

Figure 5. Time variation in (a) total fish biomass, (b) the fish population, and (c) UIA with varying anabolism rate b.

In Figure 6a, it appears that the catabolism rate due to temperature d_1 has a noticeable impact on the fish biomass. As the catabolism rate increases, the fish biomass decreases. For fish, an increase in catabolism due to higher temperatures means they require more energy to maintain their metabolic functions. If the energy intake is insufficient to meet the elevated metabolic needs, a reduction in fish biomass occurs. From Figure 6b,c, it is worth noting that the UIA and the fish numbers do not seem to be affected by any changes in the catabolism rate. The nitrogenous waste excreted by fish primarily influences UIA concentrations. Although an increase in catabolism may increase nitrogenous waste production, the direct impact of changes in catabolism rate on UIA concentration may be minimal or regulated by other factors in the aquatic environment. The number of fish in a population is influenced by reproductive rates, mortality rates, and migration patterns rather than individual metabolic rates. Changes in catabolism might affect individual fish health and growth, but do not directly cause immediate changes in fish numbers unless increased metabolic demands lead to higher mortality rates over time.

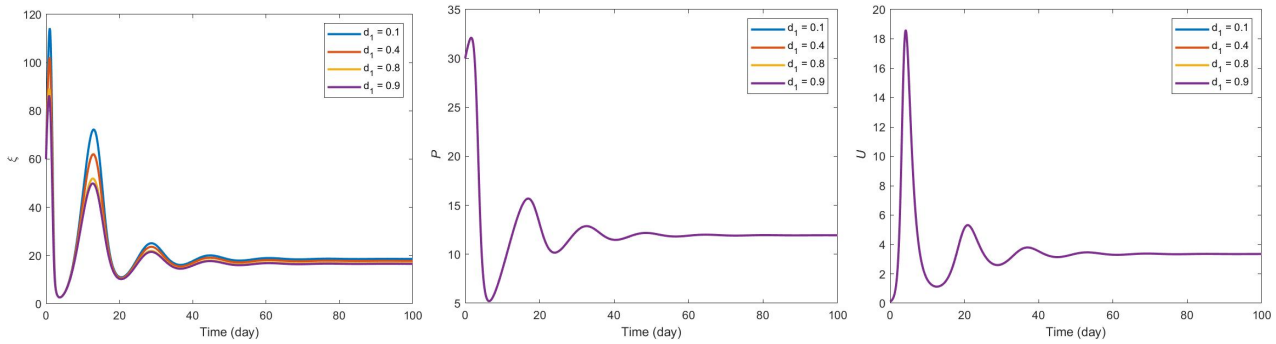

Figure 6. Time variation in (a) total fish biomass, (b) the fish population, and (c) UIA with varying catabolism rate due to temperature d_1.

Based on the simulation presented in Figure 7a, the catabolism rate, due to UIA (d_2), has a direct effect on the fish biomass. As the catabolism rate increases, the fish biomass decreases. This is because of increased metabolic stress and tissue damage. From Figure 7b,c, we note that the concentration of UIA and fish numbers remain unaffected by changes in the catabolism rate due to UIA. The concentration of UIA in the water is mostly influenced by factors such as ammonia excretion rates, water pH, and temperature. Changes in the catabolism rate d_2 do not directly alter these factors. Therefore, varying d_2 does not change the amount of UIA produced. Similarly, it does not necessarily reduce the fish population immediately because biomass measures the total mass of live fish, whereas the fish numbers count individual fish. Over time, if an increase in the catabolism rate causes significant mortality, fish populations can decline, but this is a secondary effect and not an immediate consequence of changes in d_2.

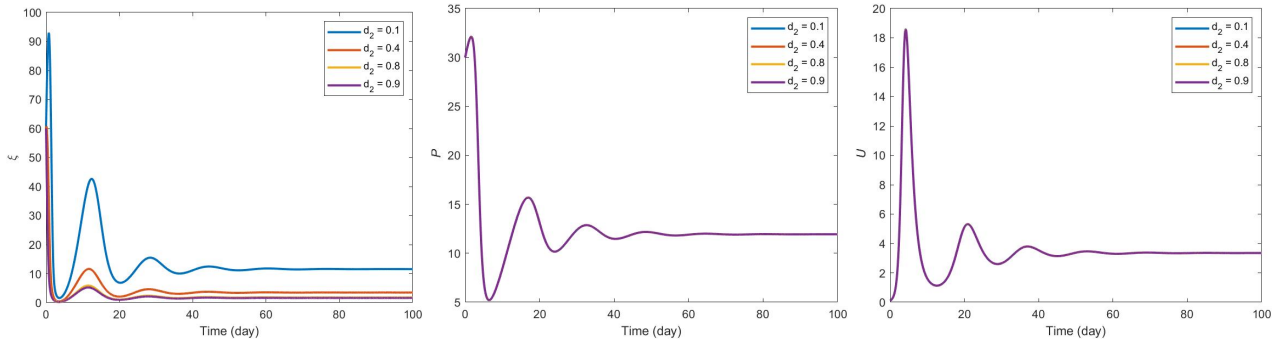

(a) **(b)** **(c)**

Figure 7. Time variation in (a) total fish biomass, (b) the fish population, and (c) UIA with varying catabolism rate due to UIA d_2.

Figure 8a shows that the population mortality rate due to UIA (d_3) directly affects the fish biomass. As the mortality rate increases, the fish biomass increases. This is because a higher mortality rate leads to a lower fish population, as demonstrated in Figure 8b; hence, density-dependent factors such as competition for food and space are reduced. Since P directly drives UIA generation, its reduction significantly lowers ammonia accumulation, as illustrated by the inverse relationship shown in Figure 8c.

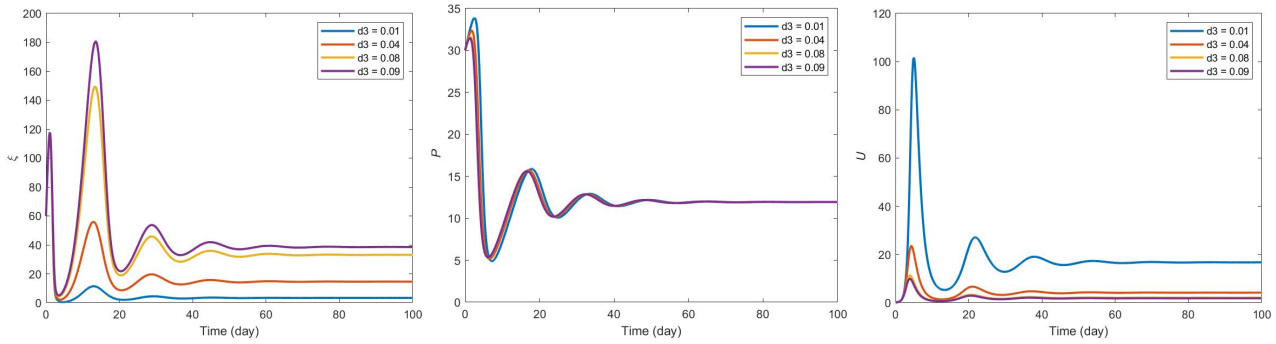

(a) **(b)** **(c)**

Figure 8. Time variation in (a) total fish biomass, (b) the fish population, and (c) UIA with a varying mortality rate of a population due to UIA d_3.

Figure 9a,b demonstrate that there is a negative correlation between the rate of UIA due to population (c_1) as well as fish biomass and number. This suggests that there is a delicate balance between the rate of UIA and fish biomass and number that must be maintained to support ecosystem health. On the other hand, Figure 9c shows a reversal of the trend observed in the previous two figures; here, c_1 and UIA concentration are positively correlated, which agrees with the expected real-world scenario.

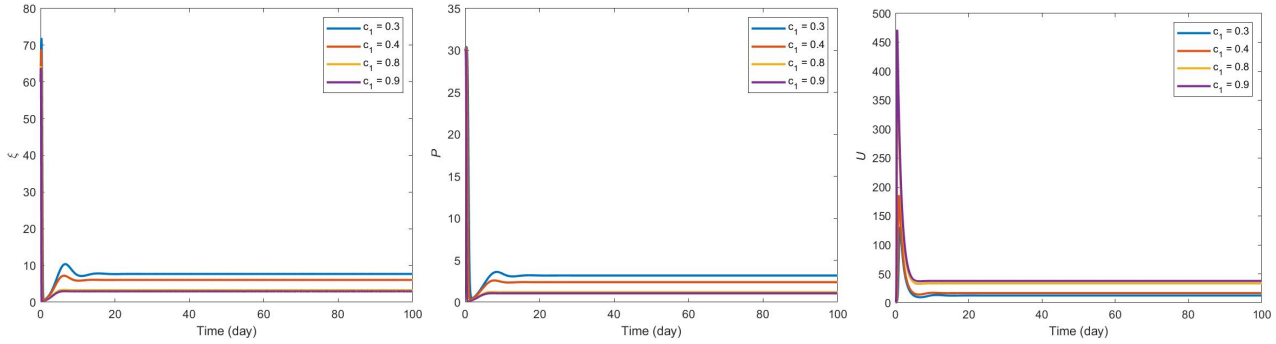

(a) **(b)** **(c)**

Figure 9. Time variation in (a) total fish biomass, (b) the fish population, and (c) UIA with varying rate of UIA due to population c_1.

The numerical results in Figure 10 illustrate the system's sensitivity to the rate of UIA due to temperature (c_2). As shown in Figure 10a, a higher c_2 leads to a marked reduction in fish biomass ξ. This agrees with the experiment presented in [22]. Figure 10b,c illustrate the impact of c_2 on biological and chemical parameters. An increase in c_2 leads to a reduction in the fish population (Figure 10b) while driving a significant increase in the concentration of UIA (Figure 10c). These observations are crucial to understanding the impact of the rate of UIA on aquatic ecosystems and for developing effective strategies to manage UIA concentration.

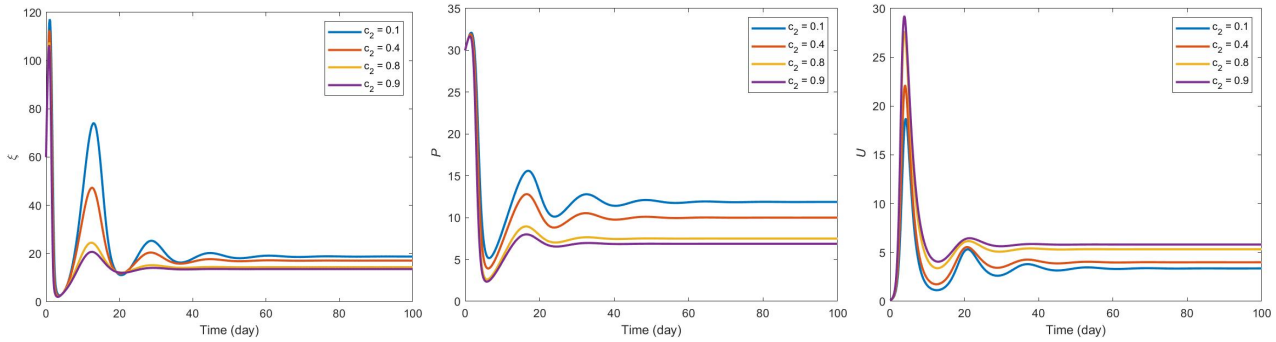

(a) **(b)** **(c)**

Figure 10. Time variation in (a) total fish biomass, (b) the fish population, and (c) UIA with varying rates of UIA due to temperature c_2.

The numerical simulations in Figure 11 illustrate the critical role of the UIA filtration rate r in maintaining system stability. As shown in Figure 11a, an increase in r facilitates a significant rise in the fish biomass ξ. This positive correlation is driven by the rapid reduction of environmental toxicity; as the filtration efficiency improves, the equilibrium concentration of U decreases sharply (Figure 11c). Figure 11b illustrates a positive correlation between the UIA filtration rate and fish population; higher filtration efficiency consistently supports greater fish numbers. Figure 11c shows that the rate of filtering UIA also affects the concentration of UIA in the water. It is evident that a lower rate of filtering UIA results in a higher concentration of UIA, which can be detrimental to the aquatic ecosystem. These findings highlight the need for proper monitoring and management of UIA filtration

systems to maintain a healthy environment.

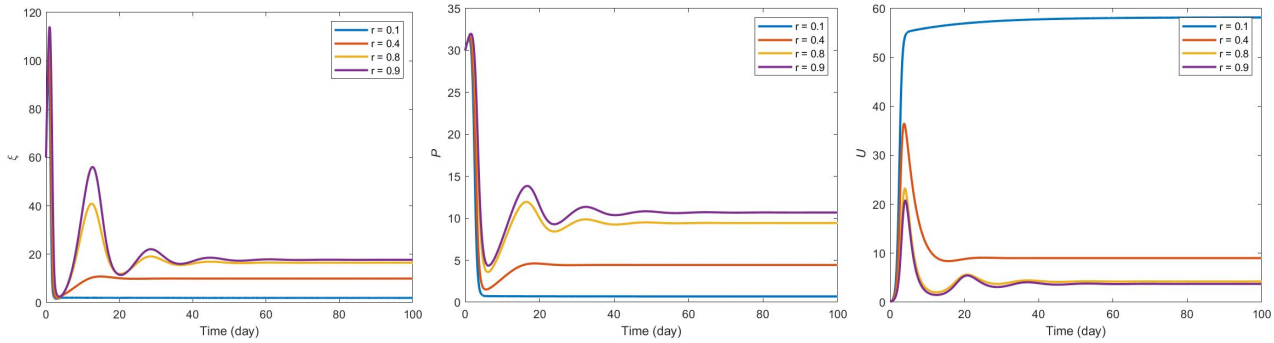

(a) **(b)** **(c)**

Figure 11. Time variation in (a) total fish biomass, (b) the fish population, and (c) UIA with varying rate of filtering UIA r.

5. UIA estimation using the MFM

We pose the following estimation problem:

EP1: Given the number of fish $P(t)$, find $U(t)$.

The MFM is proposed to solve **EP1**. First, we need to recall the definition of a modulating function (MF).

Definition 1. A function $\phi(t) \neq 0$ is considered an MF of order l on $\left[0, t_f\right]$ if it satisfies the following conditions:

$$\begin{cases} \phi(t) \in C^{(l)}\left(\left[0, t_f\right]\right), \\ \phi^{(p)}(0) = \phi^{(p)}\left(t_f\right) = 0, \quad p = 0, 1, \ldots, l-1, \end{cases} \tag{5.1}$$

where $t_f > 0$, and p represents the order of the derivative.

The MFM solution to **EP1** is provided in the next theorem.

Theorem 4. *Let $\sum_{j=1}^{J} \chi_j(t)\zeta_j$ be a basis expansion of the unknown $U(t)$ in Eq (2.1b), where $\chi_j(t)$ and ζ_j, for $j = 1, \ldots, J$, are basis functions and basis coefficients, respectively. Let $\{\phi_m(t)\}_{m=1}^{m=M}$ be a class of modulating functions of order $l \geqslant 1$ and $M \geqslant J$. Then the unknown coefficients ζ_j, $j = 1, 2, \ldots, J$, can be estimated by solving the system*

$$Az = L, \tag{5.2}$$

where the components of the $M \times J$ matrix A have the form

$$A_{mj} = -d_3 \int_0^{t_f} P(t)\phi_m(t)\chi_j(t)dt, \tag{5.3}$$

for $m = 1, \ldots, M$ and $j = 1, \ldots, J$. The components of the vector $L \in \mathbb{R}^{M\times 1}$ are

$$L_m = -\int_0^{t_f} \phi_m'(t)P(t)dt - \int_0^{t_f} p_s\phi_m(t)dt. \tag{5.4}$$

The vector z contains the unknowns ζ_j, $j = 1, 2, \ldots, J$.

Proof. STEP 1: Multiply Eq (2.1b) by a modulating function $\phi_m(t)$, which

$$\frac{\mathrm{d}P}{\mathrm{d}t}\phi_m = p_s\phi_m - d_3PU\phi_m. \tag{5.5}$$

STEP 2: Integrate Eq (5.5) over the time interval $[0, t_f]$, that is

$$\int_0^{t_f} \frac{\mathrm{d}P}{\mathrm{d}t}\phi_m dt = \int_0^{t_f} p_s\phi_m dt - \int_0^{t_f} d_3PU\phi_m dt. \tag{5.6}$$

STEP 3: Apply integration by the parts formula to the left-hand side of (5.6) and use the properties in (5.1), which provides

$$-\int_0^{t_f} P(t)\phi_m'(t)dt - \int_0^{t_f} p_s\phi_m dt = -\int_0^{t_f} d_3P(t)U(t)\phi_m dt. \tag{5.7}$$

By expressing $U(t)$ in its basis expansion and considering M MFs, Eq (5.7) can be reformulated as the linear system presented in (5.2), whose components are specified in (5.3) and (5.4). □

6. Numerical results of UIA estimation

The primary objective is to support the theoretical results given in the previous section with numerical ones for the estimation of the unionized ammonia concentration UIA and the model parameter. By applying the developed estimation algorithms and utilizing the generated data, we demonstrate how the unknown variables and parameters can be accurately identified and analyzed. The numerical simulations provide valuable insights into the performance of the proposed estimation approach under different conditions, highlighting noise-free and noisy scenarios to assess the robustness and reliability of the method. The time discretization, basis functions, modulating functions, and noisy measurements are chosen as follows:

Time discretization: The time interval is uniformly discretized using a step size $\Delta t = 10^{-4}$ and a final time $t_f = 10$.

Basis functions: Polynomial basis functions are considered, which have the form

$$\chi_j(t) = t^{j-1}, \quad j = 1, 2, \ldots, J.$$

MFs: There are various types of MFs, including polynomial, sinusoidal, Hermite, and Poisson functions [15]. We use polynomial MFs of the form:

$$\phi(t) = t^{q_1}\,(t_f - t)^{q_2}$$

where q_1 and q_2 are positive integers used as tuning parameters.

Exact measurements: We obtain our measurements by solving the model numerically as shown in Section 4.

Noisy measurement: In practice, measurements are usually noisy (not perfect). To simulate this, we add a zero-mean white Gaussian noise to the exact measurements. Noise at a level of 5% has been added to the measurements as follows:

$$\tilde{P}(t) = P(t) + \sigma\,\omega(t) \tag{6.1}$$

where $\tilde{P}$ refers to the noisy data, $\omega(t)$ is a zero-mean white Gaussian random noise, and the coefficients σ is standard deviations adjusted such that the selected noise level is obtained; that is:

$$\sigma = \frac{\text{noise level} \times \|P\|_2}{\|\omega\|_2 \times 100}. \tag{6.2}$$

These noisy measurements are then utilized to assess the method's capability to perform effectively in the presence of noise.

Figure 12 shows the exact measurement and the noisy one with 5% noise level.

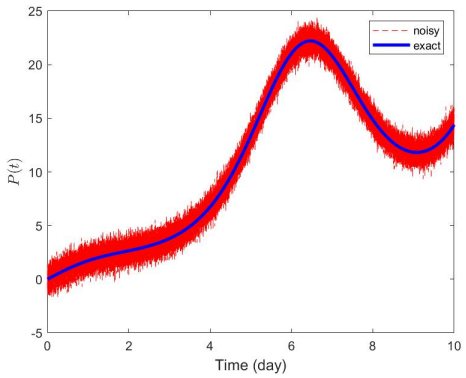

Figure 12. The exact P (blue solid line) and the noisy $\tilde{P}$ (red dashed line) after adding 5% noise, where $\sigma = 0.6251$.

(a) Noise-free data

Figure 13a illustrates the estimated UIA concentration obtained using the MFM in the noise-free case. As shown in the figure, the estimated values exhibit a very close match with the exact curve across the simulation period, confirming the high accuracy and reliability of the estimation approach. Figure 13b presents the absolute error between the exact and estimated values of UIA in noise-free case. The results show that the estimation error remains very small across the entire simulation period, with slight increases only at the time boundaries, which confirms the high accuracy of the MFM approach.

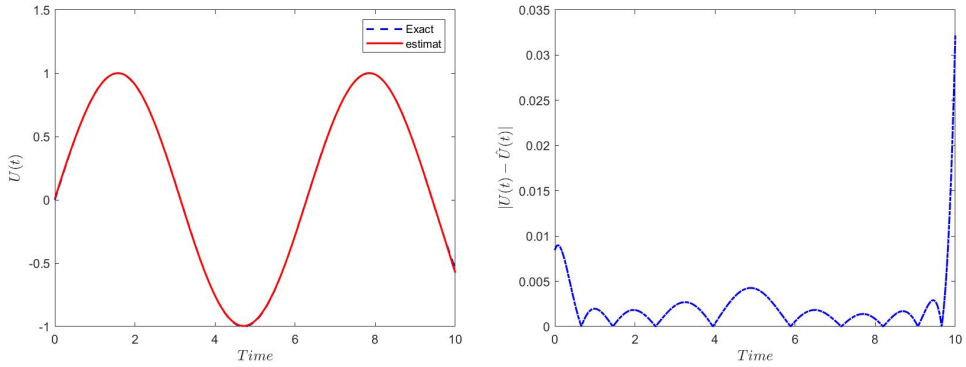

(a) (b)

Figure 13. (a) Exact UIA (blue dashed line) and the estimated one (red solid line) for the noise-free case. The MFM parameters are set as $a = 1, M = 22$, and $J = 10$. (b) Absolute error between exact UIA, $U(t)$, and the estimated one, $\hat{U}(t)$.

(b) Noisy data

The exact and estimated UIA are presented in Figure 14a. Figure 14b presents the absolute error between the exact and estimated UIA under the noisy case. The results demonstrate that the estimation error remains small throughout the simulation period, with minor increases at the time boundaries, thereby confirming the high accuracy of the MFM.

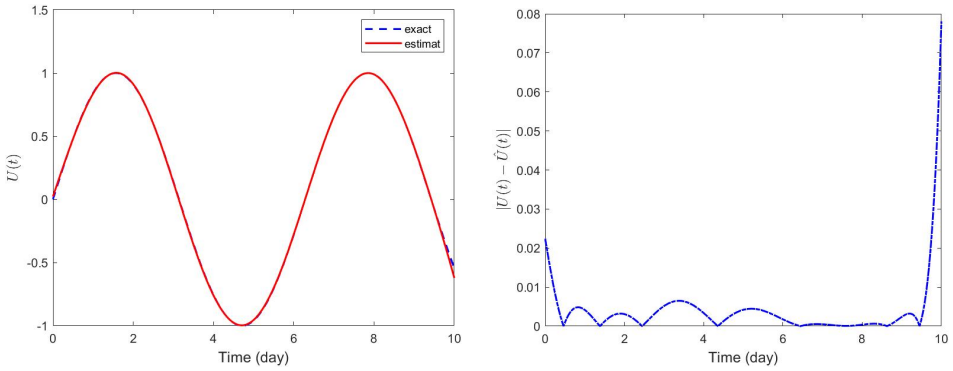

(a) (b)

Figure 14. (a) Exact UIA (blue dashed line) and the estimated one (red solid line) with noise at 5%. The MFM parameters are set as $a = 2, M = 22$, and $J = 10$. (b) Absolute error between exact UIA, $U(t)$, and the estimated one, $\hat{U}(t)$.

The relative errors in the noisy free and noisy cases are reported in Table 3. The estimation results confirm the high accuracy of the proposed approach. In the noise-free case, a very low relative error of 0.53% is recorded. When the noise level is increased to 5%, the relative error rises only slightly to 1.28%. This minimal change highlights the robustness of the MFM, which consistently delivers accurate and stable estimates of the concentration UIA, even in the presence of measurement noise.

Table 3. Relative error of UIA estimation under different noise levels.

Noise level	Relative error
Noise-free	0.53%
5%	1.28%

7. Conclusions

In this paper, we developed and analyzed a rigorous mathematical framework to study the growth of fish and the effect of water quality dynamics in aquaculture ponds, with particular attention to the role of unionized ammonia (UIA) as a critical toxicant. Our central aim was to capture the interactions between fish biomass (ξ), fish population (P), and UIA concentration, and to provide a theoretical and numerical foundation for understanding system behavior under different environmental conditions.

A bioenergetic fish growth model was developed. The model equations described the dynamics of biomass (ξ), population (P), and UIA concentration, accounting for anabolic growth, catabolic losses due to intrinsic biological activity and environmental stress, and mortality induced by ammonia accumulation. A qualitative analysis of the system was conducted, proving the positivity and boundedness of the solutions and ensuring biological realism. Equilibrium points were identified, and

their local stability was analyzed mathematically, shedding light on the long-term dynamics of the aquaculture system under steady environmental conditions. Numerical simulations were then carried out to validate the analytical results, showing consistency between theoretical predictions and computational outcomes. A sensitivity analysis was also performed, revealing the key biological and environmental parameters that exert the greatest influence on fish growth and water quality. In particular, the filtration rate parameter (r) was shown to play a central role in regulating UIA concentration: Higher values of r improved water quality and enhanced biomass and population levels, while insufficient filtration accelerated ammonia accumulation and increased mortality. This finding underlines the dual importance of filtration as a model parameter and a practical management strategy for maintaining pond stability.

In addition, the MFM was applied to estimate the UIA concentration. The proposed estimation framework successfully avoided the instability usually associated with noisy measurements. The numerical simulations confirmed that the MFM provides accurate and robust estimates under noise-free and noisy conditions, thereby offering a reliable soft-sensing tool in scenarios where direct UIA measurement is costly or unavailable.

In this paper, we provide significant advancements in modeling, estimation, and filtration of aquaculture systems. These contributions support the development of sustainable fish farming practices and align with the goals of fostering food security, environmental sustainability, and innovation in aquaculture management.

In future work, we will use real data to validate and refine the model. Such validation will enable the proposed MFM for UIA estimation to be employed as a robust soft sensor for automated water-quality control.

Author contributions

Sharefa Asiri: conceptualization, funding acquisition, supervision, software, and writing – review & editing; Salma Al-Tuwairqi: conceptualization, formal analysis, and methodology; Sara Al-Amoudi: software and writing – original draft. All authors have read and agreed to the published version of the manuscript.

Use of Generative-AI tools declaration

The authors declare they have not used Artificial Intelligence (AI) tools in the creation of this article.

Acknowledgments

The project was funded by KAU Endowment (WAQF) at King Abdulaziz University, Jeddah, Saudi Arabia. The authors, therefore, acknowledge with thanks WAQF and the Deanship of Scientific Research (DSR) for technical and financial support.

Conflict of interest

The authors declare that they have no competing interests.

References

1. FAO, The state of world fisheries and aquaculture: meeting the sustainable development goals, 2018. Available from: https://openknowledge.fao.org/handle/20.500.14283/i9540en.
2. T. Gjedrem, *Selection and breeding programs in aquaculture*, Springer, 2005. https://doi.org/10.1007/1-4020-3342-7
3. C. E. Boyd, General relationship between water quality and aquaculture performance in ponds, *Fish Dis.*, 2017, 147–166. https://doi.org/10.1016/B978-0-12-804564-0.00006-5
4. M. R. Darmawan, Y. Andriani, U. Subhan, I. Zidni, The effect of the aeration system on fish health performance in aquaponics, *J. Fish Health*, **5** (2025), 177–185. https://doi.org/10.29303/jfh.v5i2.6288
5. P. Satanwat, *Acclimatization and application of biofilters for nitrogen removal in marine recirculating shrimp culture system*, Ph. D. thesis, Thammasat School of Engineering, 2018. https://doi.org/10.58837/CHULA.THE.2018.222
6. E. Batır, Ö. Metin, M. Yıldız, O. T. Özel, D. Fidan, Sustainable land-based imta: holistic management of finfish, mussel, and macroalgae interactions, emphasizing water quality and nutrient dynamics, *J. Environ. Manage.*, **372** (2024), 123411. https://doi.org/10.1016/j.jenvman.2024.123411
7. S. Tabrett, I. Ramsay, B. Paterson, M. A. Burford, A review of the benefits and limitations of waste nutrient treatment in aquaculture pond facilities, *Rev. Aquacult.*, **16** (2024), 1766–1786. https://doi.org/10.1111/raq.12921
8. M. Flores-Iwasaki, G. A. Guadalupe, M. Pachas-Caycho, S. Chapa-Gonza, R. C. Mori-Zabarburú, J. C. Guerrero-Abad, Internet of things (iot) sensors for water quality monitoring in aquaculture systems: a systematic review and bibliometric analysis, *AgriEngineering*, **7** (2025), 78. https://doi.org/10.3390/agriengineering7030078
9. Y. Yi, A bioenergetics growth model for nile tilapia (oreochromis niloticus) based on limiting nutrients and fish standing crop in fertilized ponds, *Aquacult. Eng.*, **18** (1998), 157–173. https://doi.org/10.1016/S0144-8609(98)00028-4
10. I. Seginer, Growth models of gilthead sea bream (sparus aurata L.) for aquaculture: a review, *Aquacult. Eng.*, **70** (2026), 15–32. https://doi.org/10.1016/j.aquaeng.2015.12.001
11. J. A. Buentello, D. M. Gatlin III, W. H. Neill, Effects of water temperature and dissolved oxygen on daily feed consumption, feed utilization and growth of channel catfish (ictalurus punctatus), *Aquaculture*, **182** (2000), 339–352. https://doi.org/10.1016/S0044-8486(99)00274-4
12. Y. Yilmaz, M. Arabacİ, The influence of stocking density on growth and feed efficiency in gilthead seabream, sparus aurata, *J. Anim. Vet. Adv.*, **9** (2010), 1280–1284. https://doi.org/10.3923/javaa.2010.1280.1284
13. F. Aljehani, I. N'Doye, T. M. Laleg-Kirati, Model-based versus model-free feeding control and water-quality monitoring for fish-growth tracking in aquaculture systems, *IFAC J. Syst. Control*, **26** (2023), 100226. https://doi.org/10.1016/j.ifacsc.2023.100226

14. F. Aljehani, I. N'Doye, T. M. Laleg-Kirati, Extended kalman filter for fish weight estimation using augmented fish population growth model, *IFAC-PapersOnLine*, **56** (2023), 9855–9861. https://doi.org/10.1016/j.ifacol.2023.10.407
15. S. Asiri, *Modulating function-based method for parameter and source estimation of partial differential equations*, Ph. D. thesis, King Abdullah University of Science and Technology, 2017. https://doi.org/10.25781/KAUST-4B3A9
16. S. Asiri, S. Elmetennani, T. M. Laleg-Kirati, Moving-horizon modulating functions-based algorithm for online source estimation in a first-order hyperbolic partial differential equation, *J. Sol. Energy Eng.*, **139** (2017), 061007. https://doi.org/10.1115/1.4037743
17. S. Asiri, D. Y. Liu, Finite-time estimation for a class of systems with unknown time-delay using modulating functions-based method, *Asian J. Control*, **25** (2023), 746–757. https://doi.org/10.1002/asjc.2858
18. D. Y. Liu, O. Gibaru, W. Perruquetti, T. M. Laleg-Kirati, Fractional order differentiation by integration and error analysis in noisy environment, *IEEE Trans. Autom. Control*, **60** (2015), 2945–2960. https://doi.org/10.1109/TAC.2015.2417852
19. G. Bo, H. Wei, T. Zhang, M. Duan, D. Li, Y. Wang, et al., Acute and chronic un-ionized ammonia toxicity to 'all-fish'growth hormone transgenic common carp (cyprinus carpio L.), *Chin. Sci. Bull.*, **55** (2010), 4032–4036. https://doi.org/10.1007/s11434-010-4165-5
20. P. Khamchuai, M. Maleewong, S. Rujivan, Developed bioenergetics fish growth model for nile tilapia (oreochromis niloticus) aquacultured in wastewater treatment pond: the royal project in petchaburi, Thailand, *Proceedings of the ANSCSE16 Conference*, 2012.
21. M. Martcheva, *An introduction to mathematical epidemiology*, Springer, 2015. https://doi.org/10.1007/978-1-4899-7612-3
22. S. Barnard, M. W. V. Goethem, S. Z. de Scally, D. A. Cowan, P. J. van Rensburg, S. Claassens, et al., Increased temperatures alter viable microbial biomass, ammonia oxidizing bacteria and extracellular enzymatic activities in antarctic soils, *FEMS Microbiol. Ecol.*, **96** (2020), fiaa065. https://doi.org/10.1093/femsec/fiaa065

AIMS Press